RSC Advances

PAPER

View Article Online
View Journal | View Issue

Cite this: *RSC Adv.*, 2024, **14**, 24152

Understanding the anti-corrosion characteristics of surface modification of h-BN and carbon nanotubes/magnesium composites in simulated seawater

Victor Sunday Aigbodion, *[abc] Abdulmajeed Abdullah Alayyaf[d] and Chinemerem Jerry Ozoude[e]

Received 4th June 2024
Accepted 17th July 2024

DOI: 10.1039/d4ra04076g

rsc.li/rsc-advances

In order to address the issues of wettability and scattering between matrix and reinforcement and enhance corrosion resistance, the effects of incorporating hexagonal boron nitride (h-BN) into magnesium-carbon nanotubes (Mg-0.5 wt% CNTs) nanocomposites were successfully investigated. An inventive coating with h-BN using a novel electroless chemical deposition technique and double stir casting were used. The composites were produced by varying weight percentages of h-BN (0, 2, 4, and 6). The corrosion testing, microstructural analysis, and physical testing of the samples were carried out. A corrosion resistance of 75.1% was obtained when the 4 weight percent of h-BN content was compared to Mg-0.5% wt% CNTs. Even though the relative density increased noticeably, this was due to the uniform dispersion of h-BN nanoparticles over the entire surface. Researchers have established that adding 4 wt% h-BN to the Mg-0.5 wt% CNT nanocomposite can improve the wettability between Mg and CNTs and enhance the corrosion resistance properties.

1 Introduction

Hybrid metal matrix nanocomposites (HMMNCs) provide an exciting and promising breakthrough in the domains of materials science and engineering.[1,2] These materials are created by combining nanofibers or nanoparticles with a metal matrix to develop a composite material with enhanced properties. HMMNCs are considered the next generation of metal matrix nanocomposites (MMNCs) for advanced industrial applications due to their many advantages.[3] The addition of nanoparticles, such as CNTs, graphene, or ceramic nanoparticles, into a metal matrix can significantly enhance the mechanical properties of HMMNCs. Improved hardness, wear resistance, stiffness, corrosion, and strength are a few instances of this.[4,5] Improved stability and heat conductivity make HMMNCs suitable for high-temperature applications, such as components used in automobiles and aircraft. Because HMMNCs reduce material weight without sacrificing strength, they are useful in areas where weight reduction is essential, such as in the aircraft and automotive industries.[6]

Applications like electromagnetic shielding or electronic packaging can benefit from HMMNCs' specific electrical and magnetic properties.[7] Certain high-molecular-weight nanocomposite materials (HMMNCs) have the potential to provide enhanced corrosion resistance in harsh environments, such as offshore projects.[8] Nanoparticles improve the tribological (wear and friction) and corrosion properties of HMMNCs. This means that they can be used in places where corrosion is a problem, like in bearings and other mechanical parts.[9] Several industries, including aerospace, automotive, electronics, energy, and more, use HMMNCs.[10] They have a lot of potential for usage in highly performance-demanding, cutting-edge technological applications. As technology and materials science advance, HMMNCs are anticipated to play a critical role in supplying materials with enhanced performance and customisable characteristics that meet the demands of complex industrial applications.

To fully achieve the promise of these state-of-the-art materials, scientists and engineers continue to explore new combinations and manufacturing techniques. Several industries, particularly the automotive and aerospace sectors, are showing a great deal of interest in magnesium metal matrix composites. Magnesium metal matrix composites are becoming an indispensable material in industrial applications due to their exceptional properties that outperform those of conventional

[a]*Faculty of Engineering and the Built Environment, University of Johannesburg, P. O. Box 534, Auckland Park, South Africa. E-mail: victor.aigbodion@unn.edu.ng*
[b]*Department of Metallurgical and Materials Engineering, University of Nigeria, Nsukka Postal Code 410001, Nsukka, Nigeria*
[c]*Africa Centre of Excellence, ACESPED University of Nigeria, Nsukka Postal Code 410001, Nsukka, Nigeria*
[d]*Department of Chemistry, College of Sciences, King Saud University, Riyadh 11451, Saudi Arabia*
[e]*Department: Materials Science and Engineering, University of North Texas, Denton, Texas, USA*

materials.[11] Mg metal matrix composites combine the benefits of carbon fibres and ceramics with the lightweight nature of magnesium to address the pressing need for high-performance materials in a range of industrial applications.[12] Of these reinforcements, carbon nanotubes (CNTs) have garnered the most attention due to their exceptional properties and capacity to dramatically improve the performance of magnesium metal matrix composites.[13] The addition of CNTs significantly improves the mechanical properties of the Mg metal matrix composites. Adding CNTs to the Mg matrix makes it stronger and harder, creating a network of reinforcements that effectively stops dislocation movement.[14] In addition to mechanical improvements, the combination of CNTs with Mg-matrix produces noticeable benefits in terms of thermal and electrical conductivity.[15] Consequently, researchers have recently conducted numerous investigations to enhance the mechanical, corrosion, tribological, and physical properties of magnesium metal matrix composites by incorporating carbon nanotubes (CNTs) as reinforcements using diverse production techniques.[16] For instance, Goh *et al.*[17] used the powder metallurgy technique to create magnesium-CNT composites containing 00.3 wt% CNTs. They found a 25% increase in tensile strength compared to pure magnesium. Upadhyay *et al.*[18] investigated Mg-based composites reinforced with 4 weight percent CNTs. They concluded that the Mg/0.4 wt% CNTs composites enhanced their tensile strength. According to Zhang *et al.*,[19] the Mg/0.5 wt% CNTs produced by the electrophoretic deposition process exhibited a tensile strength improvement of around 35%. Yakup *et al.*[20] studied the corrosion properties of CNTs in Mg and discovered that adding more CNTs below 0.2 wt% made the material more resistant to corrosion. This was because the CNTs grouped together and spread out. Naing *et al.*[21] mixed Mg with 0.3 and 1.3 wt% CNTs and tested how fast it corroded in simulated seawater. They found that the higher rate of corrosion was caused by microgalvanic action between the Mg matrix (anodic) and the CNTs (cathodic). Saberi *et al.*[22] and Hiroyuki *et al.*[23] found that the galvanic effect plays a vital role in the corrosion of carbon nanotubes and the AZ31B magnesium alloy. The literature above reveals that the increased corrosion rate of Mg and CNTs stems from the microgalvanic interaction between the anodic Mg matrix and the cathodic CNTs, which occurs when the CNTs exceed 0.2 wt%. We endeavored to boost the CNT percentage to 0.5% by coating the CNTs with h-BN, thereby improving their uniform distribution within the Mg matrix. Adding h-BN as a reinforcing ingredient to Mg matrix composites (MMCs) has potential, because of its low coefficient of friction and ability to lubricate itself, h-BN is an attractive addition to MMCs. High temperature settings or vacuum conditions, which restrict the use of traditional liquid lubricants, greatly benefit from the self-lubricating properties of h-BN.[24,25]

According to a review of the literature, no one has looked into what happens when h-BN is added to Mg/CNTs/h-BN hybrid composites. These composites combine the benefits of h-BN in the Mg matrix[25] and CNTs.[26,27] This combination makes the material perfect for usage in both industrial and automotive applications. The point of this study is to find out how h-BN and nano-sized CNTs influence the microstructure, densification, and corrosion resistance of Mg/0.5 wt%/(0–6 wt%) h-BN composites made by double stir casting. The electroless deposition of Ni onto the surfaces of h-BN and CNTs significantly improved the wettability between the reinforcements and the Mg matrix.

2 Materials and method

In this study, Mg-0.5 wt% CNTs was used as a base to make hybrid composites that were strengthened with h-BN particles at 0, 2, 4 and 6 wt%. The experimental protocols employed a two-fold stir casting procedure to yield hybrid composites with a Mg-0.5 wt% CNT/h-BN.

2.1 Materials

In Lagos State, Nigeria, an electrical firm produced magnesium ingots with 99.99% purity as a matrix. Rice husks were obtained in Ebonyi State, Nigeria; the nanoshell h-BN, with an average particle size of 70–80 nm and a purity of 99%, was obtained in JoelChem, Nigeria.

2.2 Method

2.2.1 Production of CNTS from rice husks. Researchers developed carbon nanotubes (CNTs) with a thickness of 15 nm using rice husk. The solvent self-ignition temperature method converts rice husk (RH), a paddy residue, into carbon nanotubes (CNTs). The rice husks (RH) were washed, cleaned with deionized water, and dried for eight hours at 100 °C. After being reduced to a fine powder, the dry RH was sieved to a 65 μm particle size. Ethanol was used to dissolve the catalyst, ferrocene, and the dry RH. The mixture was covered with an aluminium sheet. The samples were placed in the quartz tube's core and heated using a Samsung microwave oven model M539 MAN200405W, which has a 700 W power output and operates at 2.55 GHz. The produced carbon nanotubes were sonicated for two hours in a water bath after being suspended in 60 millilitres of concentrated HNO_3 and H_2SO_4 solution in a 3 : 1 ratio. After that, the refined CNTs were rinsed many times with distilled water and let to dry at 110 °C for 24 hours.[28,29]

2.2.2 Surface modification of h-BN and CNTs. The surface particles of h-BN and CNTs were coated using the electroless process to improve the bonding between the matrix and the reinforcements. The two primary procedures in the electroless nano-Ag coating technique that were used to deposit nano-Ag on the surfaces of either h-BN or CNTs were sensitization and nano-Ag deposition. The h-BN and CNTs are immersed in a 10% sodium hydroxide solution and vigorously agitated for one hour, after which they are immersed in acetone for an additional hour to enhance their surface sensitivity and effectively remove any surface contaminants. Following that, distilled water was used to wash the h-BN and CNTs after they had been filtered and dried in electric furnace at 110 °C for an hour.

The bath's solution, which included 300 mL L^{-1} of formaldehyde and 3 g L^{-1} of silver nitrate, was adjusted to a pH of 12 using ammonia. As soon as formaldehyde was introduced, the

reaction began. After 10 minutes of room temperature magnetic spinning, the solution containing h-BN and CNTs was suspended. The electroless process was successfully finished in less than half an hour. After filtering, acetone was used to clean the mixture. After that, it was vacuum-dried at 110 °C for an hour.[27] The electroless chemical deposition technique coats h-BN or CNTs with 30 percent Ni. To finish this procedure, the predicted amounts needed are 80 gL^{-1} potassium sodium tartrate, 100 gL^{-1} nickel chloride, 50 gL^{-1} ammonium chloride, and 100 gL^{-1} sodium hypophosphite. A temperature of around 100 degrees Celsius and a pH of approximately 9.2 are established. The liquid is then combined with different amounts of ceramic powder.[11]

2.2.3 Mg-CNT/h-BN composite nanoparticles manufacturing. To develop the Mg-CNTs/h-BN hybrid nanocomposite, the double stir casting technique described below was used. The bottom of the graphite crucible was filled with 0.5 wt% CNTs with varying weight percentages of *x*h-BN ($x = 0$, 2, 4, and 6 wt%). The projected weight of the magnesium ingot was then charged, heated to 750 degrees Celsius, and steeped for 30 minutes in an argon atmosphere. Once the molten metal had fully melted, degassing tablets (hexachloroethane) were used to reduce porosity. To stir the molten metal twice at a speed of 250 rpm, a stainless steel-coated graphite stirrer was employed, and it was lowered progressively into the melt. The material was then put into a mould that had been heated to 500 °C for 30 minutes in order to achieve uniform solidification. The sample was machined after casting in order to determine its mechanical and physical properties.

2.2.4 Characteristics of Mg-CNTs/h-BN hybrid nano composites. The density of the sintered hybrid composite samples was calculated using the Archimedes principle in compliance with MPIF Standard 42, 1998. Both air and distilled water were used for measurements prior to determining the samples' densities. The samples' morphological composition was examined using a scanning electron microscope (SEM). To prepare the hybrid composite samples for microstructure examination, they were first ground using fine-grit paper and then polished with alumina paste. X-ray diffraction (XRD) analysis with Cu k radiation ($\lambda = 0.15406$ nm) was used to look into the structure of the phases in the samples. The polished hybrid composite samples in the United States underwent a Vickers hardness instrument test. For every sample, the mean of five readings was selected at random. A dwell time of 15 seconds and an applied load of 300 g of hardness were used. Electrochemical experiments utilising the model CHI660D electrochemical (CH Instrument, USA) equipment were used to determine the corrosion behaviour. A standard three-electrode electrochemical cell was used for the studies. The surface area of the specimen, measured in centimeters, served as the working electrode, while platinum (Pt) served as the counter electrode and AgCl model C2015B1-5 (China) served as the reference electrode. The electrodes were immersed in simulated saltwater in a 250 mL beaker. For 3600 seconds—the amount of time required for the open circuit potential (OCP) to approach a quasi-stationary state—the OCP data was determined. A scan rate of 0.5 mV s^{-1} was used to assess polarisation. A 10 mV small-amplitude AC pulse, ranging in frequency from 0.1 Hz to 0.5 MHz, impressed the EIS. The electrochemical parameters, such as the corrosion potential (E_{corr}), corrosion current density (i_{corr}), and corrosion rate, were computed using Tafel plots. The impedance data was then examined using Nyquist plots. Analysis was done on the parameters derived from the best similar circuit. Eqn (1) was used to calculate the polarisation resistance.[18]

$$R_p = \frac{\beta_a \beta_c}{2.3 i_{corr}(\beta_a + \beta_c)} \quad (1)$$

where; anodic constant = β_a, current density = i_{corr}, cathodic constant = β_c

3 Results and discussion

3.1 Al-CNTs/h-BNH hybrid composite density

The density of casted Mg-CNT-based hybrid composites was calculated using Archimedes' principle, and the theoretical density was estimated using the role of the mixture. Fig. 1 displays the relative density of the Mg-0.5 wt% CNT hybrid nanocomposites reinforced with different weight percent h-BN ratios of 0, 2, 4, and 6. It shows a consistent increase in density as the h-BN ratio increases. The greater densities of h-BN and Mg, at 2.1 and 1.78 g cm^{-3}, respectively, may be attributed. Additionally, the great it's also important that the CNTs and h-BN are spread out evenly in the magnesium matrix. This is possible because the nano-Ag and Ni coatings on surface keep them almost 99.5% of the casted Mg matrix densified. This is in consistent with the work of ref. 30.

3.2 Microstructure

Fig. 2 and 3 displays the samples' microstructures at various h-BN levels. Fig. 2 and 3 show that the Mg granules are unevenly distributed, specifically, when compared to one another, the grains on the left side of the surface are bigger than the ones on the right. Furthermore, it is evident that the distribution of grains varies along the surface. With the addition of h-BN at a 2% level, the microstructure somewhat improved. This is due to the h-BN addition, which reduced the particle size relative to the unreinforced sample and almost uniformized the particle

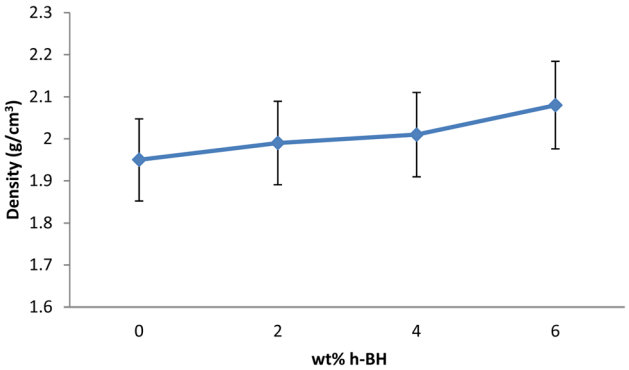

Fig. 1 Variation of density with wt% h-BN content.

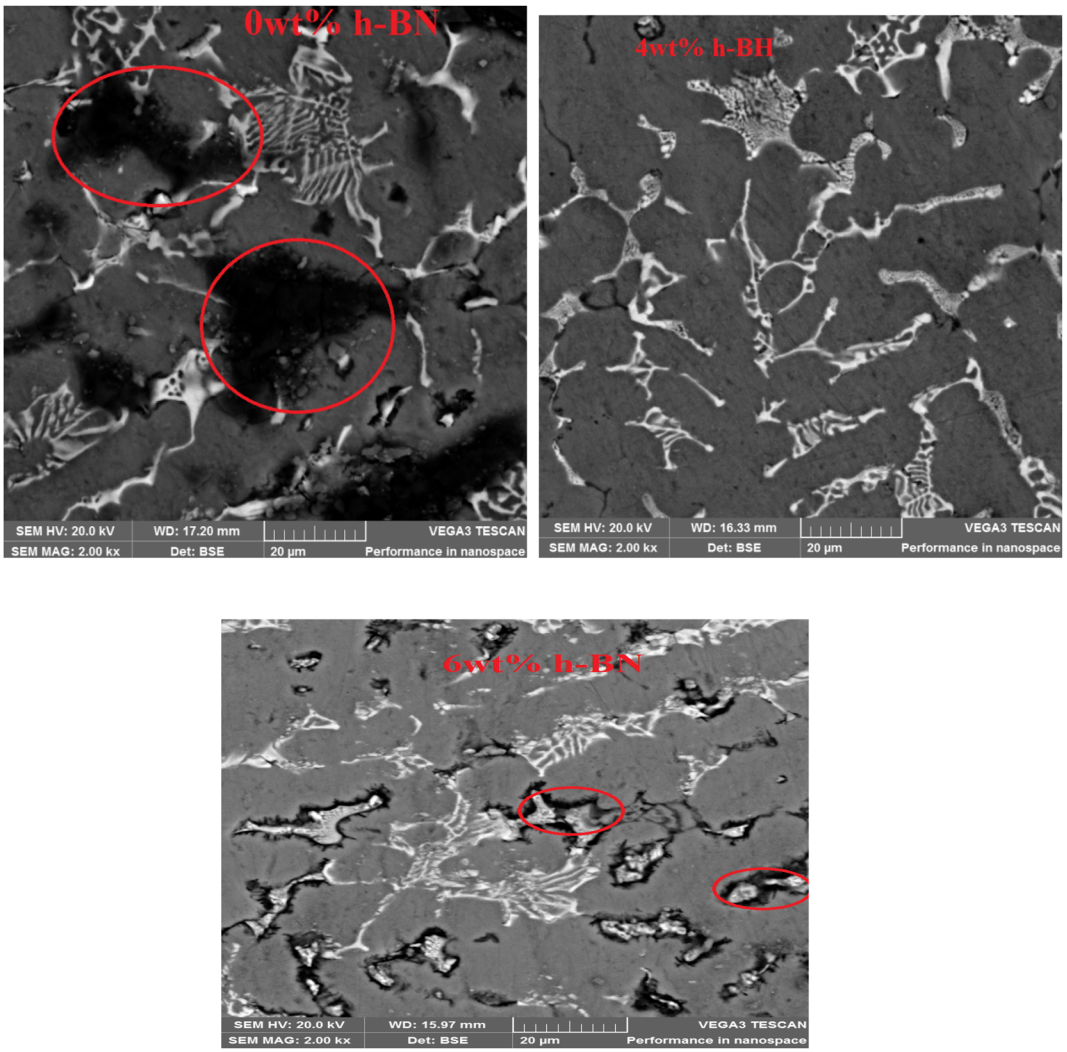

Fig. 2 The SEM images of the casted Mg-0.5 wt% CNTs/h-BN nanohybrid composites reinforced with the 0, 4 and 6 wt% of nano h-BN.

distribution. It is notable that the h-BN addition prevented the grains from becoming larger and helped to coordinate and organize them. An important finding is the uneven distribution of Ag and Ni grains among the Mg and h-BN grains which is visible as white phases in the microstructure. The distribution of Mg particles at 4% h-BN was more uniform when the particle size decreased; compared to 2% h-BN. Ag and Ni grains are emerging in addition to the Mg and CNT nanoparticles. Notably, despite the absence of pores in the section with 2% h-BN, a few of them appeared on the surface in a dense way. Fig. 2 shows that as the percentage of h-BN increases to 4%, the size and distribution of the grains become smaller and more uniform compared to their previous proportion. Furthermore, we see that at a percentage of 4% h-BN, the best plastic formation and dynamic recrystallization are clearly visible. Two main factors were responsible for this observation: 1. h-BN reduced the number of microscopic holes by making it easier for the granules to slide over one another. 2. The addition of Ag and Ni coatings reduces internal holes and enhances granule adhesion,[30] as the h-BN percentage increases to 4%, Fig. 3 illustrates how plastic formation and dynamic recrystallization occur, producing small grains and regularity in the particles. There were even amounts of nickel and silver grains on and between the carbon nanotube, h-BN, and magnesium, which made the size and pores smaller. Fig. 2 and 3 show that when the wt% h-BN goes up to 6, there is less wettability, which makes more porosity or voids by making it harder for particles to pack together and move around. The reason for this was that the thickness of the molten metal prevented the CNTs and h-BN's in the Mg matrix from becoming improperly wettable. In the work of,[31,32] the stir casting method yielded similar results.

3.3 Phase analysis by XRD

Fig. 4 displays an X-ray diffraction (XRD) study of a magnesium-0.5 wt% carbon nanotube (CNT) nanocomposite. It was evidence that at 45 and 61°, in all these samples, this corresponded to α-Mg and CNTs phases. However, there is an absence of h-BN phases in the XRD spectrum of 0 wt% h-BN. The presence of h-BN phases was obtained in the composites of 2, 4, and 6 wt% h-BN at 73 and 80°, respectively. No chemical

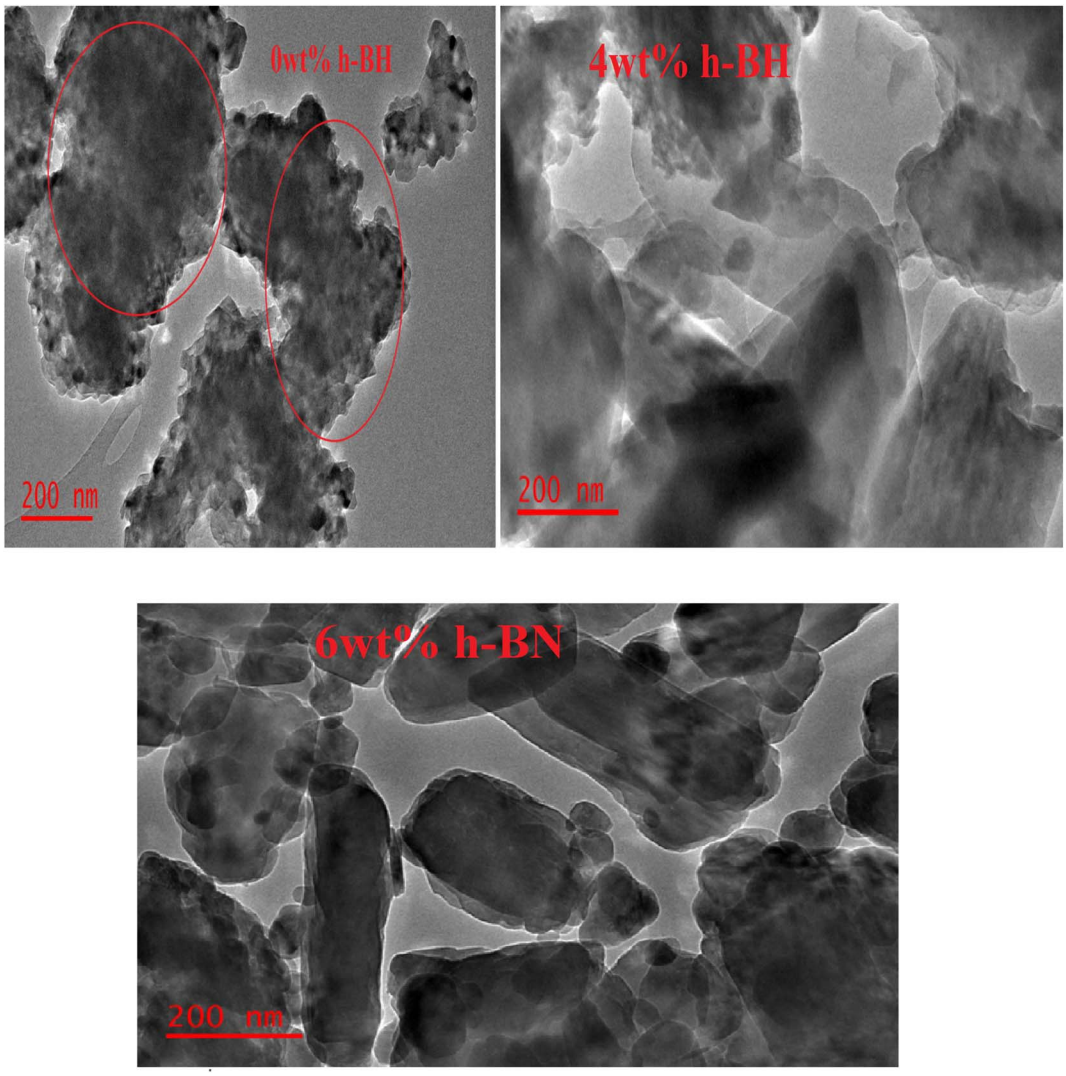

Fig. 3 The TEM images of the casted Mg-0.5 wt% CNTs/h-BN nanohybrid composites reinforced with the 0, 4 and 6 wt% of nano h-BN.

precipitation happened when the Ag and Ni particles were deposited, which shows proper bonding between the Mg, CNTs, and h-BN. The recognised peaks for Mg, CNTs, and h-BN, which show no undesirable new phases, indicate that the casting conditions were under control. The crystallite size generally decreases with an increase in coated h-BN weight, with the exception of 6 wt% h-BN.

3.4 Corrosion behaviour

3.4.1 Open circuit potential. The samples were submerged in a 3.5% NaCl solution at 25 °C, and their anticorrosion performance was evaluated using open circuit potential (OCP) testing. Fig. 5 illustrates the cathodic corrosion shielding effect of the sample. The production of surface oxides and other corrosion products was linked to the Mg-CNTs-4% h-BNs somewhat higher OCP, and hence a higher potential value was obtained with samples with h-BN addition. The Mg-0.5 wt% CNTs samples containing h-BN exhibited higher noble potential values compared to the Mg-0.5 wt% CNTs. This difference can be attributed to h-BN acting as a protective mechanism against corrosion of the Mg-0.5 wt% CNTs. As a result of this event, OCP values shift, moving towards a nobler state. This is especially noticeable in the Mg-0.5 wt% CNTs-4% h-BN sample, which suggests improved protective qualities. Moreover, we observed the impact of h-BN concentration on the OCP of the Mg-0.5 wt% CNTs over the 3600 seconds immersion time, and the OCP remained constant, indicating the achievement of a steady-state potential. However, we observed OCP variations in other samples during the 3600 seconds time period, suggesting the potential for stabilisation through further testing.

3.4.2 Tafel curves for potentiodynamic polarisation. Tafel measurements, or linear potentiodynamic polarisation, were used to examine the protective qualities of casted Mg-0.5 wt% CNTs/h-BN nanohybrid composites reinforced with 0, 2, 4, and 6 wt% of nano h-BN in a 3.5% NaCl solution. Fig. 6 and Table 1 display key polarisation characteristics such as the corrosion potential (E_{corr}), the corrosion rate (CR), and the current density (i_{corr}). Tafel graphs showing the corrosion behaviour of casted

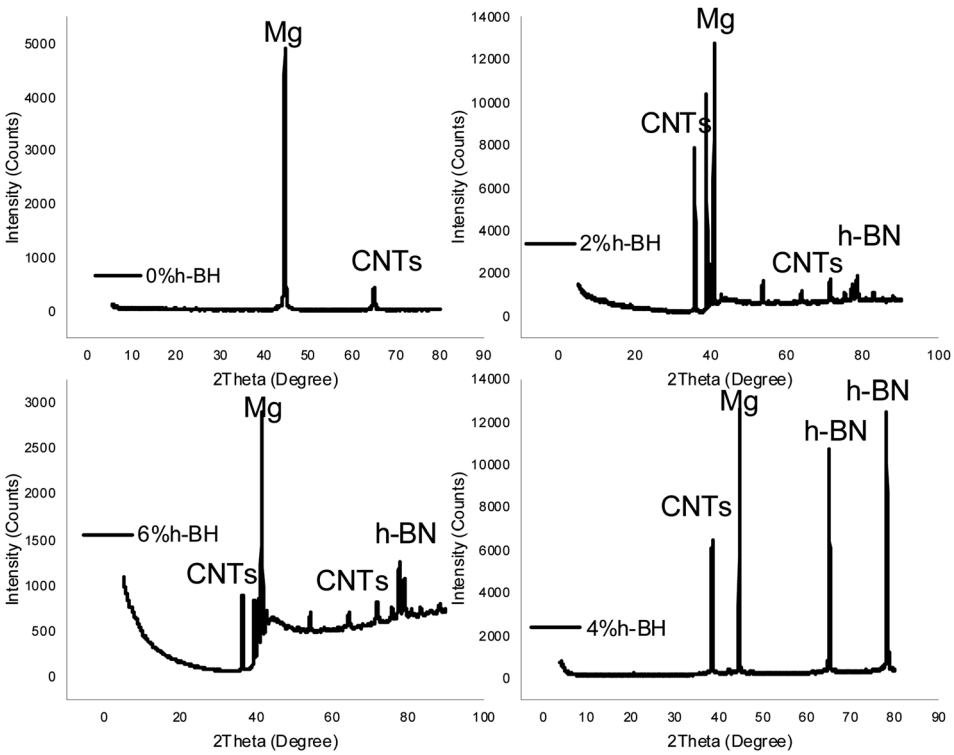

Fig. 4 The XRD analysis of the casted Mg-0.5 wt% CNTs/h-BN nanohybrid composites reinforced with the 0, 2, 4, and 6 wt% of nano h-BN.

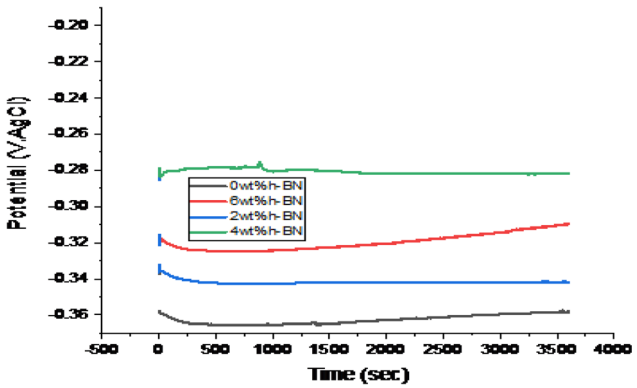

Fig. 5 OCP curves of the casted Mg-0.5 wt% CNTs/h-BN nanohybrid composites reinforced with the 0, 2, 4, and 6 wt% of nano h-BN.

Mg-0.5 wt% CNTs/h-BN nanohybrid composites reinforced with 0, 2, 4, and 6 wt% of nano h-BN composite are shown in Fig. 6. This method made it easier to evaluate how well various h-BN films protected against corrosion. Significantly, as Fig. 6 shows, the polarisation curves of the with-h-BN and without-h-BN samples showed clear variances, indicating different corrosion behaviours among the materials examined.

When compared to the Mg-0.5 wt% CNTs/0% h-BN, the corrosion resistance of the samples h-BN significantly improved, as shown by a shift in corrosion potential (E_{corr}) towards a more noble positive potential and a decrease in corrosion current (i_{corr}). This enhancement is usually ascribed to the protective function of the h-BN, which shields the sample surface and encourages a positive shift in E_{corr} and i_{corr}. This protective mechanism in composite coatings is linked to barrier and passivation effects. The correlation between corrosion resistance and potential underscores the importance of corrosion current density in determining the corrosion rate. Interestingly, the sample with 4% h-BN showed increased resistance to corrosion. The Mg-0.5 wt% CNTs/0 wt% h-BN sample showed the greatest values for corrosion rate (CR), corrosion current density (i_{corr}), and low polarisation resistance (R_p),

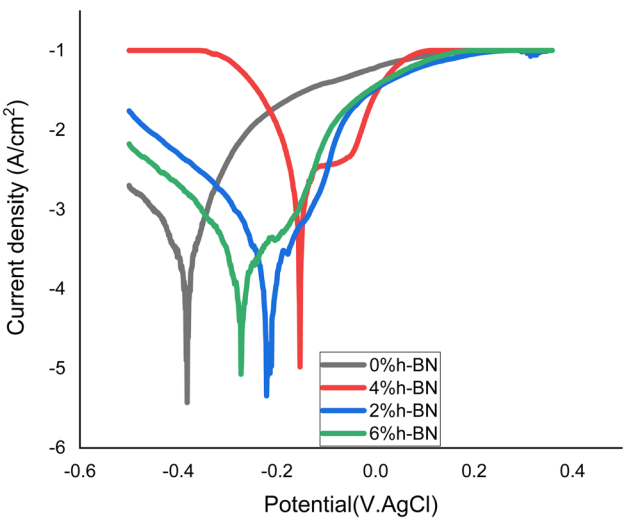

Fig. 6 Tafel curves of the casted Mg-0.5 wt% CNTs/h-BN nanohybrid composites reinforced with the 0, 2, 4, and 6 wt% of nano h-BN.

Table 1 Tafel and EIS results of the casted Mg-0.5 wt% CNTs/h-BN nanohybrid composites reinforced with the 0, 2, 4, and 6 wt% of nano h-BN

h-BN (wt%)	i_{corr} (A cm^{-2})	E_{corr} (V)	Polarisation resistance (Ω)	Corrosion rate (MPY)	R_{ct} (Ω cm^2)	C_{pdl} (μF cm^{-2}) × 10^{-4}	CPE × 10^{-4} Ω^{-1} s^n cm^{-2}	$X^2 \times 10^{-4}$
0	3.57×10^{-3}	−0.37	35	17.07	8.24	1000.13	5.6	3
2	1.94×10^{-3}	−0.29	101	9.68	9.46	701.38	3.4	2
4	3.10×10^{-4}	−0.19	145	3.35	11.00	473.45	2.1	1
6	1.71×10^{-3}	−0.27	108	8.71	9.80	688.65	3.2	2

demonstrating its lower corrosion resistance in the corrosive medium (3.5% NaCl) (Table 1).

The Mg-0.5 wt% CNTs with h-BN, on the other hand, greatly increased R_p while decreasing CR and i_{corr}. This shows that the h-BN particles are effectively blocking the entry of chloride ions. Reductions in CR and i_{corr} readings indicate that the 4% h-BN sample performed better than the 0% h-BN. This better performance is believed to be due to increased adhesive strength, potentially preventing gaps or holes from forming in the sample. In addition, it's possible that the inclusion of 4% h-BN in the matrix minimised their sizes and boundaries and stopped micro-voids in samples, all of which improved corrosion resistance. On the other hand, a higher concentration of 6% h-BN would encourage the development of bigger grain boundaries, providing more channels for the penetration of chloride ions and raising the values of CR and i_{corr}. Furthermore, compared to findings obtained without h-BN, the inclusion of h-BN lowers passivation current and oxide monomer current density, suggesting the production of a less conductive composite with enhanced protective qualities.[19]

Lower corrosion current and higher maximum polarisation resistance are the results of adding h-BN, which suggests improved protective qualities.[27] It is well known that barrier effects and electrochemical protection are the two main components that enhance corrosion resistance in composites. Electrochemical protection mechanisms, stated differently, justify the establishment of a passive layer on the sample surface and the increase in corrosion potential. This results in a reduction of the corrosion current density and, therefore, a percentage drop in the composite's corrosion rate.

Fig. 6 illustrates how the Mg-0.5 wt% CNTs/0% h-BN composite's corrosion potential shifted towards the anodic region in contrast to the addition of h-BN. It was evidence that the dispersion degree of CNTs in the matrix, the cathodic properties of CNTs, and the galvanic couplings between the Mg and CNTs are the factors that affect the corrosion resistance of Mg/0.5 wt% CNTs composites. The addition of h-BN formed during the creation of magnesium matrix composites reinforced with carbon nanotubes (CNTs) and potential variations are significant factors influencing the corrosion resistance of these materials. Combining h-BN with magnesium hydroxide in a α-phase composite undergoing corrosion results in the production of a passive layer with a sizable surface area. This characteristic stops chloride ions from piercing sample surfaces, slowing down the pace of corrosion. However, the oxide layer that turned into metal chloride is broken down by the presence of chlorine ions. This causes magnesium $(OH)_2$ to convert into magnesium chloride, which accelerates in the Mg-0.5 wt% CNTs/0% h-BN composites.[33–35]

3.4.3 Electrochemical impedance spectroscopy (EIS). EIS was used to confirm how well the composites under investigation prevented corrosion when immersed in a 3.5% NaCl solution. The EIS spectra of the Nyquist and Bode plots of the cast Mg-0.5 wt% CNTs/h-BN nanohybrid composites that were strengthened with 0, 2, 4, and 6% wt% nano h-BN samples can be seen in Fig. 7. The corrosion process's charge transfer is explained by the single capacitive loop shown in the Nyquist plots. The diameter of the loops grows as the wt% h-BN rises 4. The diameter of the circle increases much more with the addition of h-BN, suggesting that the increased electrode surface covering by h-BN is the cause of the composite increased resistance.[36] This suggests that the impedance of the composite rises. It was observed that the semicircle diameter of the sample with h-BN is larger than the sample without h-BN. Higher corrosion resistance is often indicated by a sample with a bigger semicircle diameter or more impressive persistence of charge transfer.[13] The decrease in corrosion rate seen when charge transfer resistance increases are thought to be caused by the corrosion products generated at the sample surface.[24,34]

As the percentage of h-BN increased to 4, the overall impedance arc diameter increased significantly in the sample. The sample with 4% h-BN had the largest capacitive arc width, which meant it was the best at protecting against corrosion. Comparing the sample without h-BN addition makes this clear. The corrosion enhancement of the h-BN was attributed to the formation of a barrier between the corrosive electrolyte and the sample surface; the resultant oxide layer passively increased the materials' resistance to corrosion.

There is an obvious semi-circle loop showing the formation of an oxide layer; a bigger radius of the semi-circle indicates a more powerful protection efficacy of the passive layer that is created. Likewise, peel-off in the passive layer may be inferred by the inductance loop. Fig. 8 illustrates how the impedance plots are fitted using an analogous circuit with a single time constant.

Solution resistance (R_s) and double layer capacitance (C_{dl}), which are connected in parallel to the charge transfer resistance (R_{ct}), are components of the analogous circuit. Since the metal/solution contact does not equate to an ideal capacitor, CPE is swapped by double layer capacitance, C_{dl}, to get a more accurate

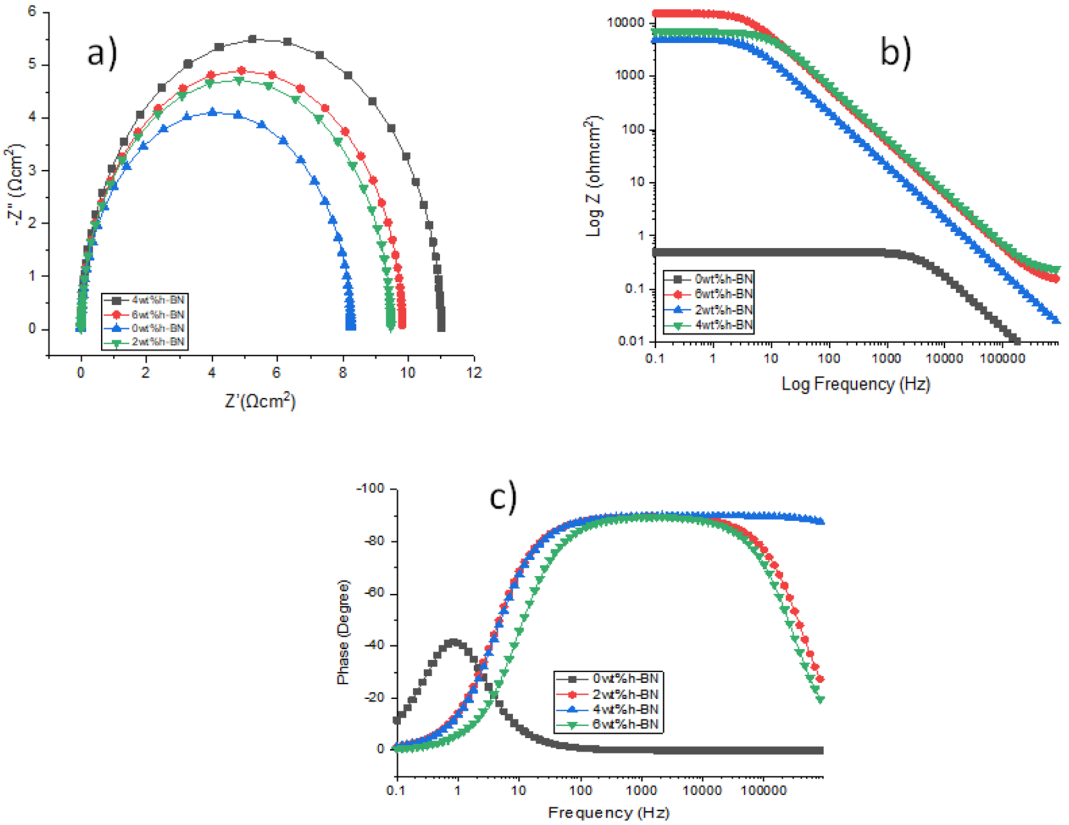

Fig. 7 (a) Nyquist plots (b) Bode impedance plots (c) Bode phase angle plots of the casted Mg-0.5 wt% CNTs/h-BN nanohybrid composites reinforced with the 0, 2, 4, and 6 wt% of nano h-BN.

semicircle fit. A CPE's impedance may be found in the following expression (eqn (2)):

$$Z_{\mathrm{CPE}} = \frac{1}{Z_0(\mathrm{j}w)^n} \tag{2}$$

The CPE magnitude is represented by Z_0, the imaginary number j is equal to the square root of -1, the angular frequency is represented by w in rad s^{-1}, and the phase shift, which is associated with the double layer's inhomogeneities, is represented by n. The formula where $w_{\max}$ is the maximum frequency at which the imaginary component of the impedance has a maximum may be used to get the C_{dl} for a circuit that includes CPE (eqn (3)).

$$C_{\mathrm{dl}} = Z_0(w_{\max})^{n-1} \tag{3}$$

Table 1 provides the EIS parameters. R_{ct} and C_{dl} are the primary parameters derived from EIS data. In general, a drop in C_{dl} values accompanied by a rise in R_{ct} values indicates that the enhanced surface coverage and corrosion prevention performance in the solution. The resulting Bode diagrams confirm the enhanced h-BN effect as visualised by Nyquist plots. While the Bode phase angle diagram shows a more negative value of the phase angle at high frequency with increasing wt% h-BN, the Bode modulus diagram shows an increase in the impedance modulus over the whole frequency range. The resistance to the transfer of charge (R_{ct}) value, also known as the barrier that the passive layer offers for the transport of charge, may be used to assess the efficacy of the passive layer in this situation.[37,38] Greater R_{ct} values suggest that more excellent corrosion resistance is attained by decreased ion movement in the passive layer during the deterioration operation. As shown in Fig. 8a, the 0% h-BN composite has smaller semi-conductive loops than the h-BN samples, which may indicate that the h-BN has better passive layer-created obstacle efficiency. The chi-square (x^2) values were used to verify that the equivalent circuit fitted to the specification. An optimal fit is often indicated by values of x^2 between 10^{-3} and 10^{-5}.[39,40] The suggested equivalent circuit yielded relatively modest ($<1 \times 10^{-3}$) x^2 values (Table 1), indicating that the obtained impedance spectra suited the suggested equivalent circuit well.

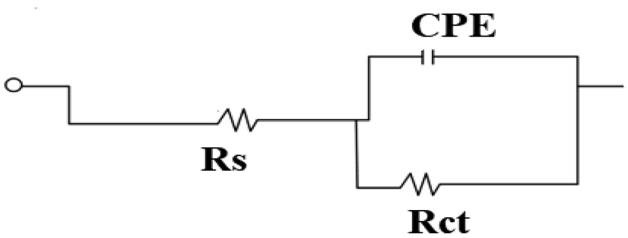

Fig. 8 Equivalent circuit model used to fit the impedance data.

3.4.4 Evaluation of the samples corroded. A SEM was used to analyze the corroded surfaces of the composite covering (see Fig. 9). It was shown that the Mg-0.5 wt% CNTs/0% h-BN samples exhibited a higher tendency to pit than the h-BN samples. There were several pits encircled, indicating that pit formation continued throughout the exposure time and accumulated on the surface (Fig. 9a). The Mg-0.5 wt% CNT sample produced the greatest number of corrosion sites, which may be attributed to microgalvanic activity between the cathodic CNTs and the anodic Mg matrix. The h-BN material's degraded surface showed that the h-BN ingredients had successfully stuck to the surface to fend against corrosion attack. The samples were encased in h-BN, which formed a passive corrosion barrier. The h-BN composite samples' hard phases provided protection against corrosive action by reducing the amount and kind of surface damage. The Mg-0.5 wt% CNTs/4% h-BN specimens, in particular, showed very little overall damage, highlighting the function of h-BN in preventing sample degradation. Furthermore, the efficient dispersion of h-BN hindered the corrosion process. This helped to close the pores and limit the paths that electrolytes and corrosive ions might take.

Atomic force microscopy (AFM) in contact mode was used to further assess the corrosion surface roughness. Fig. 10 displays typical AFM pictures of the corroded surface, the findings demonstrated that the sample of 4 wt% h-BN had higher average surface roughness values, which suggests the existence of passive films and corrosion product. For example, mean roughness values of 1.7, 2.4, 5.2 and 3.5 nm were obtained at 0, 2, 4 and 6 wt% h-BN, respectively. The findings support earlier research of,[40–43] which showed that surface roughness rose with the formation of passive films. The reason why 4 wt% h-BN sample with a greater level of roughness is considered superior for corrosion resistance of the samples.

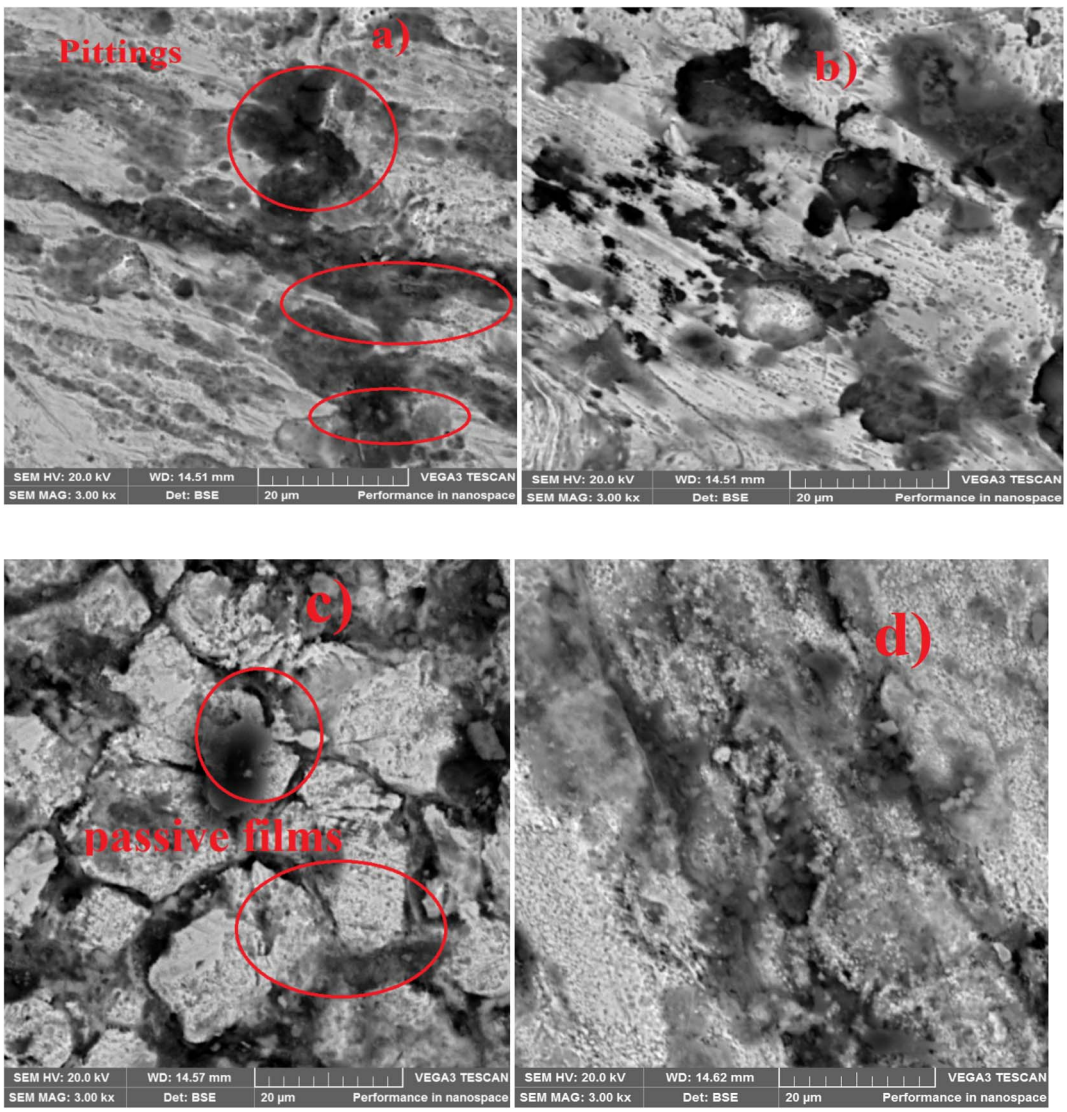

Fig. 9 SEM Corroded surface of casted Mg-0.5 wt% CNTs/h-BN nanohybrid composites reinforced with the (a) 0, (b) 2, (c) 4, and (d) 6 wt% of nano h-BN.

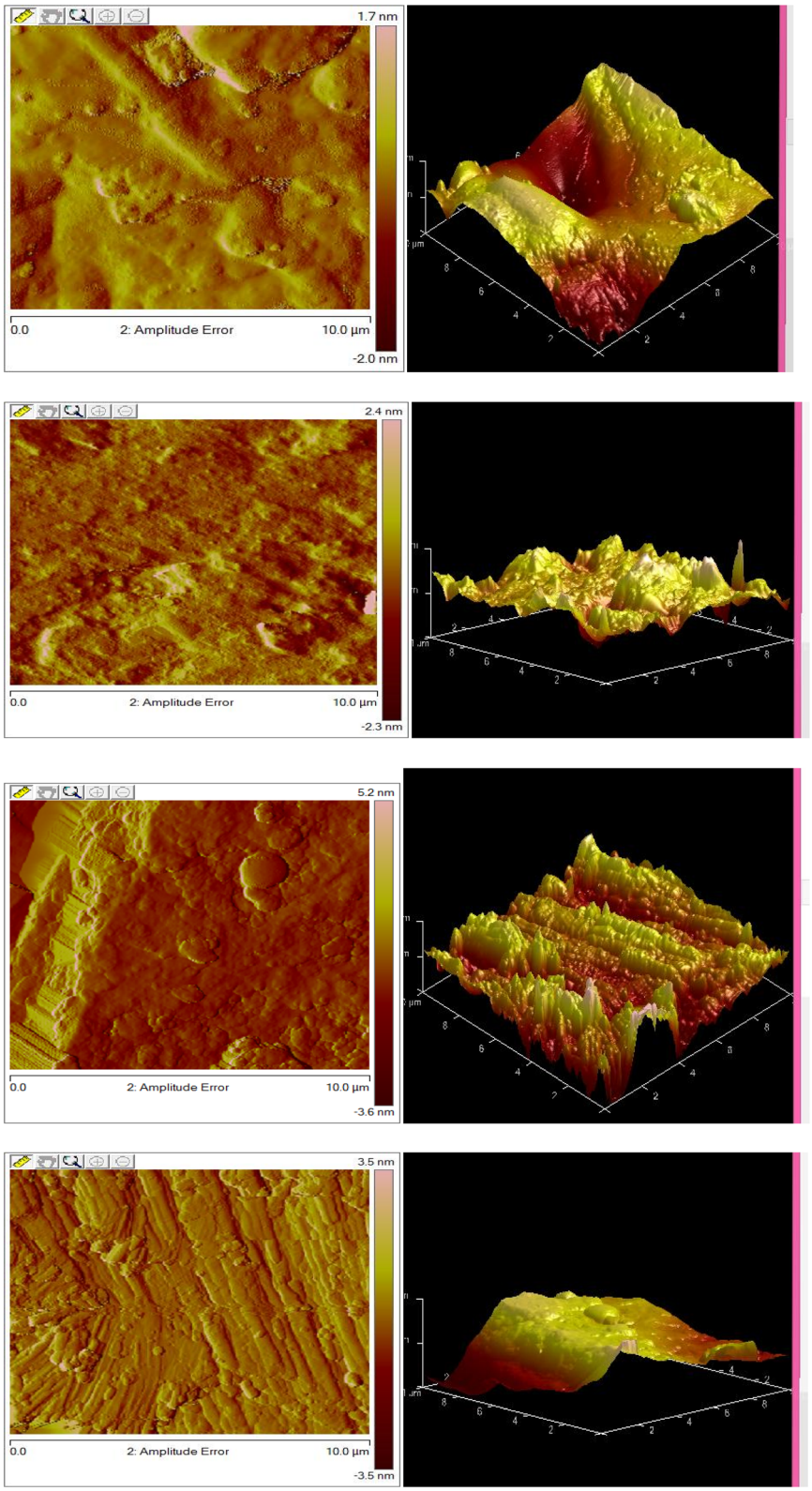

Fig. 10 (a): AFM Corroded surface of casted Mg-0.5 wt% CNTs/0 wt% h-BN nanohybrid composites. (b): AFM Corroded surface of casted Mg-0.5 wt% CNTs/2 wt% h-BN nanohybrid composites. (c): AFM Corroded surface of casted Mg-0.5 wt% CNTs/4 wt% h-BN nanohybrid composites. (d): AFM Corroded surface of casted Mg-0.5 wt% CNTs/6 wt% h-BN nanohybrid composites.

4 Conclusions

The first attempt to cover magnesium-carbon nanotubes (Mg-0.5 weight percent CNTs) with hexagonal boron nitride (h-BN) was investigated. This was done using a new electroless chemical deposition method that mixed silver (Ag) and nickel (Ni). To improve the wettability and dispersion between the reinforcement and matrix, it must overcome a number of obstacles, such as: (i) rising temperatures; (ii) high pressure; and (iii) corrosion rates. Consequently, we use the double stir casting process to mix different quantities of BN (2, 4, and 6 weight percent). Numerous microstructure, physical, and corrosion studies were conducted to look into the innovative features and attributes. The conclusions drawn from the observations and information gathered in this research may be summed up as follows:

(1) Coated h-BN nanoparticles were successfully and uniformly distributed throughout the magnesium matrix, up to a 4 weight percent concentration. However, upon increasing the h-BN level to 6 weight percent, observable particle agglomeration occurred.

(2) The effective dispersion of h-BN and CNTs throughout the matrix may lead to synergistic processes that improve corrosion resistance.

(3) At a 4 weight percent h-BN concentration, we found corrosion protection of 75.1%. A well-balanced dispersion of h-BN inside the Mg matrix cultivates improved interfacial connections and structural resilience, resulting in optimal corrosion. This concentration significantly reduces the potential negative impacts of excessive h-BN agglomeration and porosity, which leads to the highest corrosion resistance.

(4) The Mg-0.5 wt% CNTs/4 wt% h-BN nanocomposite had amazing and unique properties that showed how well this new method improved the material's resistance to corrosion and lowered the microgalvanic effect of the Mg and CNTs.

Data availability

The author confirm that the data supporting this study's conclusions is included in the publication.

Author contributions

Study conception, design, data collection, analysis and interpretation of results by Victor Sunday Aigbodion, funding of the research by Abdulmajeed Abdullah Alayyaf and draft manuscript preparation by Chinemerem Jerry Ozoude. All authors reviewed the results and approved the final version of the manuscript.

Conflicts of interest

There is no conflict of interest in this work.

Acknowledgements

The authors would like to extend their sincere appreciation to the Researchers Supporting Project (RSPD2024R527), King Saud University, Riyadh, Saudi Arabia.

References

1 T. Xin, S. Tang, F. Ji, L. Cui, B. He, X. Lin, X. Tian, H. Hou, Y. Zhao and M. Ferry, Phase transformations in an ultralight BCC Mg alloy during anisothermal ageing, *Acta Mater.*, 2022, **239**, 118248, DOI: 10.1016/j.actamat.2022.118248.

2 K. B. Nie, X. J. Wang, K. K. Deng, X. S. Hu and K. Wu, Magnesium matrix composite reinforced by nanoparticles – A review, *J. Magnesium Alloys*, 2021, **9**(1), 57–77, DOI: 10.1016/j.jma.2020.08.018.

3 Y. Yao and L. Chen, Processing of B4C Particulate-reinforced Magnesium-matrix Composites by Metal-assisted Melt Infiltration Technique, *J. Mater. Sci. Technol.*, 2014, **30**(7), 661–665, DOI: 10.1016/j.jmst.2014.06.005.

4 Z. Zeng, M. Zhou and M. Esmaily, Corrosion resistant and high-strength dual-phase Mg–Li–Al–Zn alloy by friction stir processing, *Commun. Mater.*, 2022, **3**, 18, DOI: 10.1038/s43246-022-00245-3.

5 C. O. Muga and Z. W. Zhang, Strengthening Mechanisms of Magnesium-Lithium Based Alloys and Composites, *Adv. Mater. Sci. Eng.*, 2016, 1078187, DOI: 10.1155/2016/1078187.

6 X. Li, F. Guo, Y. Ma, L. Jiang, H. Lai, H. Liu, D. Zhang and R. Pei, Rolling texture development in a dual-phase Mg-Li alloy: The role of temperature, *J. Magnesium Alloys*, 2023, **11**(8), 2980–2990, DOI: 10.1016/j.jma.2021.10.005.

7 K. Sun, Y. Zhu, Z. Li, L. Li, H. Ji and X. Lv, Fabrication of Composites with Excellent Mechanical Properties Based on Cubic Boron Nitride Reinforced with Carbon Nanotubes, *Ceram. Int.*, 2019, **45**, 14287–14290, DOI: 10.1016/j.ceramint.2019.04.138.

8 X. Yang, T. Zou, C. Shi, E. Liu, C. He and N. Zhao, Effect of Carbon Nanotube (CNT) Content on the Properties of in-Situ Synthesis CNT Reinforced Al Composites, *J. Mater. Sci. Eng. A*, 2016, **660**, 11–18, DOI: 10.1016/j.msea.2016.02.062.

9 P. Kosbe, P. Patil, M. Manickam and G. Ramamurthy, Effect of Hexagonal Boron Nitride (hBN) Inclusion on Thermal Characteristics of Disc Brake Friction Composites, *Diamond Relat. Mater.*, 2020, **107**, DOI: 10.1016/j.diamond.2020.107895.

10 E. B. Moustafa, Hybridization Effect of BN and Al_2O_3 Nanoparticles on the Physical, Wear, and Electrical Properties of Aluminum AA1060 Nanocomposites, *Appl. Phys. A*, 2021, **127**, 724.

11 S. Rathinasabapathy; M. S. Santhosh and M. Asokan, Significance of Boron Nitride in Composites and Its Applications, in *Recent Advances in Boron-Containing Materials*, IntechOpen, 2020.

12 G. Pürçek, T. Savaşkan, T. Küçükömeroğlu and S. Murphy, Dry sliding friction and wear properties of zinc-based alloys, *Wear*, 2002, **252**(11–12), 894–901, DOI: 10.1016/s0043-1648(02)00050-9.

13 S. Kamrani, D. Hübler, A. Ghasemi and C. Fleck, Enhanced Strength and Ductility in Magnesium Matrix Composites Reinforced by a High Volume Fraction of Nano- and Submicron-Sized SiC Particles Produced by Mechanical

Milling and Hot Extrusion, *Materials*, 2019, **12**(20), 3445, DOI: 10.3390/ma12203445.

14 B. J. Wang, D. K. Xu, X. Cai, Y. X. Qiao and L. Y. Sheng, Effect of rolling ratios on the microstructural evolution and corrosion performance of an as-rolled Mg-8 wt%Li alloy, *J. Magnesium Alloys*, 2021, **9**(2), 560–568, DOI: 10.1016/j.jma.2020.02.020.

15 J. Zhu, J. Qi and D. Guan, Tribological behaviour of self-lubricating Mg matrix composites reinforced with silicon carbide and tungsten disulfide, *Tribol. Int.*, 2020, **146**, 106253, DOI: 10.1016/j.triboint.2020.106253.

16 (*a*) S. Jayasathyakawin and M. Ravichandran, Fabrication and wear behaviour of Mg-3 wt% Al-*x* wt% SiC composites, *Heliyon*, 2023, **9**(2), e13679, DOI: 10.1016/j.heliyon.2023.e13679; (*b*) Y. Lailun Ni'mah and Z. Hidayatul Muhaiminah, Suprapto Suprapto Synthesis of Silica Nanoparticles from Sugarcane Bagasse by Sol–Gel Method, *Nanoparticle*, 2023, **4**(1), 10.

17 C. S. Goh, J. Wei, L. C. Lee and M. Gupta, Development of novel carbon nanotube reinforced magnesium nanocomposites using the powder metallurgy technique, *Nanotechnology*, 2005, **17**(1), 7–12, DOI: 10.1088/0957-4484/17/1/002.

18 G. Upadhyay, K. K. Saxena, S. Sehgal, K. A. Mohammed, C. Prakash, S. Dixit and D. Buddhi, Development of Carbon Nanotube (CNT)-Reinforced Mg Alloys: Fabrication Routes and Mechanical Properties, *Metals*, 2022, **12**, 1392, DOI: 10.3390/met12081392.

19 X. Zhang, L. Zou, J. Chen, P. Dai and J. Pan, Design and Preparation of CNTs/Mg Layered Composites, *Materials*, 2022, **15**(3), 864, DOI: 10.3390/ma15030864.

20 Y. Say, O. Guler and B. Dikici, Carbon nanotube (CNT) reinforced magnesium matrix composites: The effect of CNT ratio on their mechanical properties and corrosion resistance, *J. Mater. Sci. Eng. A*, 2020, **798**, 139636, DOI: 10.1016/j.msea.2020.139636.

21 N. Naing Aung, W. Zhou, C. Sim Goh, S. M. L. Nai and J. Wei, Effect of carbon nanotubes on corrosion of Mg-CNT composites, *Corros. Sci.*, 2010, **52**(Issue 5), 1551–1553, DOI: 10.1016/j.corsci.2010.02.025.

22 A. Saberi, M. S. Baltatu and P. Vizureanu, The Effectiveness Mechanisms of Carbon Nanotubes (CNTs) as Reinforcements for Magnesium-Based Composites for Biomedical Applications: A Review, *Nanomaterials*, 2024, **14**, 756, DOI: 10.3390/nano14090756.

23 H. Fukuda, J. A. Szpunar, K. Kondoh and R. Chromik, The influence of carbon nanotubes on the corrosion behaviour of AZ31B magnesium alloy, *Corros. Sci.*, 2010, **52**(Issue 12), 3917–3923, DOI: 10.1016/j.corsci.2010.08.009.

24 P. H. Shreenivasaiah, T. Gowda, B. Kuldeep, K. P. Ravikumar and K. P. Muthanna, Experimental Investigation of Cubic Boron Nitride Reinforced Al2014 Composites, in *Proceedings of the Materials Today: Proceedings*, Elsevier Ltd, 2021, vol. 46, pp. 7760–7763.

25 B. K. Kaushik and M. K. Majumder, Carbon Nanotube Based VLSI Interconnects: Analysis and Design. SpringerBriefs, *Appl. Sci. Technol.*, 2015, 1–86, DOI: 10.1007/978-81-322-2047-3.

26 Z. Wang, R. T. Qu, S. Scudino, B. A. Sun, K. G. Prashanth, D. V. Louzguine-Luzgin, M. W. Chen, Z. F. Zhang and J. Eckert, Hybrid Nanostructured Aluminum Alloy with Super-High Strength, *NPG Asia Mater.*, 2015, **7**, 1–8, DOI: 10.1038/am.2015.129.

27 M. Yildirim, D. Özyürek and M. Gürü, Effect of Milling Time on Dry Sliding Wear Behaviors of Carbon Nanotubes Reinforced Al Matrix Composites, *J. Nanosci. Nanotechnol.*, 2019, **20**, 2633–2638, DOI: 10.1166/jnn.2020.17177.

28 P. Ako, V. Aigbodion and C. Mbohwa, Understanding Asbestos Free Brake-Pad: Using Carbon Nanotube derived from waste rice husk, in *14th International Conference on Industrial Engineering and Operations Management*, 2024, DOI: 10.46254/AN14.20240014.

29 U. U. Orji, P. A. Patricia and V. S. Aigbodion, Development of polymer/carbon nanotubes incorporated sustainable materials for manufacturing of autobrake pad, *Int. J. Adv. Manuf. Technol.*, 2024, DOI: 10.1007/s00170-024-13536-5, in press.

30 M. Hasan Ali and R. Islam Rubel, A comparative review of Mg/CNTs and Al/CNTs composite to explore the prospect of bimetallic Mg-Al/CNTs composites, *AIMS Mater. Sci.*, 2020, **7**(3), 217–243, DOI: 10.3934/matersci.2020.3.217.

31 V. S. Aigbodion and I. C. Ezema, Multifunctional A356 alloy/PKSAnp composites: Microstructure and mechanical properties, *Def. Technol.*, 2020, **16**(Issue 3), 731–736, DOI: 10.1016/j.dt.2019.05.017.

32 Y. Ding, Y. Zhang, Z. Li, C. Liu, H. Wang, X. Zhao, X. Zhang, J. Xu and X. Guo, Strengthening and Toughening CNTs/Mg Composites by OpTimizing the Grinding Time of Magnesium Powder, *Nanomaterials*, 2022, **12**(23), 4277, DOI: 10.3390/nano12234277.

33 P. Pradeep Kumar, A. Raj Bharat, B. Sesha Sai, R. J. Phani Sarath, P. Akhil, G. Pradeep Kumar Reddy, *et al.*, Role of microstructure and secondary phase on corrosion behavior of heat treated AZ series magnesium alloys, *Mater. Today: Proc.*, 2019, **18**, 175–181, DOI: 10.1016/j.matpr.2019.06.291.

34 J. Satish and K. G. Satish, Preparation of magnesium metal matrix composites by powder metallurgy process, *IOP Conf. Ser.: Mater. Sci. Eng.*, 2018, **310**, 012130, DOI: 10.1088/1757-899X/310/1/012130.

35 J. Subramanian, S. Seetharaman and M. Gupta, Processing and Properties of Aluminum and Magnesium Based Composites Containing Amorphous Reinforcement: A Review, *Metals*, 2015, **5**, 743–762, DOI: 10.3390/met5020743.

36 S. Abazari, A. Shamsipur, H. R. Bakhsheshi-Rad, A. F. Ismail, S. Sharif, M. Razzaghi and F. Berto, Carbon Nanotubes (CNTs)-Reinforced Magnesium-Based Matrix Composites: A Comprehensive Review, *Materials*, 2020, **13**(19), 4421, DOI: 10.3390/ma13194421.

37 K. Funatsu, H. Fukuda, R. Takei, J. Umeda and K. Kondoh, Quantitative evaluation of initial galvanic corrosion behavior of CNTs reinforced Mg–Al alloy, *Adv. Powder Technol.*, 2013, **24**(Issue 5), 833–837, DOI: 10.1016/j.apt.2013.02.002.

38 M. K. Yu, K. O. Se, M. J. Kim, J. W. Hwang, B. Y. Yoon and H. S. Kwon, Carbon Nanotube/Magnesium Composite as a Hydrogen Source, *J. Nanosci. Nanotechnol.*, 2015, **15**(11), 8837–8841, DOI: **10.1166/jnn.2015.11527**.

39 S. M. Adams, S. A. Yaro, M. Abdulwahab and E. E. Oguzie, Extract Of Combretum Micranthum As Corrosion Inhibitor For Al–Si–Mg Alloy In Simulated Sea Water Environment, *Niger. J. Technol.*, 2016, **35**(4), 888–894, DOI: **10.4314/njt.354.1199**.

40 H. Lgaz, S. S. Kr, A. Chaouiki, K. S. Bhat, P. B. Shubhalaxmi, I. H. Ali and M. I. Khan, Ill-Min Chung, Exploring the potential role of pyrazoline derivatives in corrosion inhibition of mild steel in hydrochloric acid solution: Insights from experimental and computational studies, *Constr. Build. Mater.*, 2020, **233**, 117320.

41 V. Saraswat, M. Yadav and I. B. Obot, Investigations on ecofriendly corrosion inhibitors for mild steel in acid environment: Electrochemical, DFT and Monte Carlo Simulation approach, *Colloids Surf., A*, 2020, **599**, 124881.

42 C. W. Onyia, B. A. Okorie, N. I. Amalu and S. I. Neife, Effects Of Sulphur Addition On Microstructural Modification and Mechanical Properties of Sand Cast Al-12 wt% Si Alloy, *Niger. J. Technol.*, 2014, **33**(1), 43–48, DOI: **10.4314/njt.331.747**.

43 F. Bakare, S. Okonzuwa, A. Carlos and E. Akhabue, Effect Of Paint-Bake Like Treatment On Mechanical Properties Of Mg–Zn–Ca Alloy, *Niger. J. Technol.*, 2017, **37**(1), 124–129, DOI: **10.4314/njt.371.1585**.